Engineering Structures 206 (2020) 110034

Contents lists available at ScienceDirect

Engineering Structures

journal homepage: www.elsevier.com/locate/engstruct

Evaluation of design modifications for enhanced repairability of reinforced concrete walls

Stephen W. Blount[a], Keri L. Ryan[b,*], Richard S. Henry[c], Yiqiu Lu[c], Kenneth J. Elwood[c]

[a] WSP USA, 33301 Ninth Ave. S., Federal Way, WA 98003-2600, USA[1]
[b] Department of Civil and Environmental Engineering, University of Nevada Reno/MS 0258, 1664 N. Virginia St., Reno, NV 89557, USA
[c] Department of Civil Engineering, University of Auckland, Private Bag 92019, Auckland 1142, New Zealand

ARTICLE INFO

Keywords:
Reinforced concrete wall
Lightly-reinforced wall
Debonded reinforcement
Fiber-reinforced concrete
Engineered cementitious composite
Repairability

ABSTRACT

As a consequence of recent earthquakes in New Zealand, many concrete buildings have been demolished due to structural damage. Observations of damage to concrete walls led to substantial research and revisions to design standards to ensure that a satisfactory ductile response was achieved. However, even when the current performance objectives of the design standards are met, reinforced concrete walls may still require extensive or costly post-earthquake repairs. The objective of this project was to evaluate simple modifications to conventional reinforced concrete walls to increase their repairability. Four modified walls were constructed and subjected to cyclic lateral in-plane loading until failure, and compared to a previously tested conventional ductile reinforced concrete benchmark wall that failed at 2.5% drift. The modifications considered included debonding of reinforcement at the wall base, substituting fiber-reinforced concrete (FRC) for conventional concrete, and substituting engineered cementitious composite (ECC) for conventional concrete in the ends of the plastic hinge region (applied in two walls). Debonding delayed vertical reinforcement buckling, but failure occurred shortly thereafter (2.5% drift) due to constricted movement of the buckled bars within the debonding sleeves. The FRC and both ECC walls had increased crack propagation up to a drift demand of 0.5%, but then the cracks localized to a single dominant crack and the walls failed at drifts lower than the benchmark wall (about 1.5%). Modifications of the tested details are recommended for future test programs that investigate the repairability of concrete walls.

1. Introduction

Recent earthquakes in New Zealand have resulted in significant damage to and demolition of modern reinforced concrete (RC) structures [1–3]. RC walls have been the focus of significant research following the 2010/2011 Canterbury earthquakes, both due to the undesirable damage observed in a few modern RC wall buildings and their popularity in building construction during the rebuild. RC wall research following the Canterbury earthquakes has predominantly focused on improving the design standards for new walls to increase the reliability of achieving ductile response [4–6]. However, the damage resulting from the conventional ductile RC walls will still require significant post-earthquake repair. In reality, many structures that were only lightly damaged in the Canterbury Earthquakes were also demolished for various reasons including insurance policies, uncertainly regarding residual capacity, and the cost of repairs [7]. Nonetheless, to prepare for a better future outcome, it is pertinent to consider from a technical standpoint whether and how to repair these structures to sufficiently restore their lateral capacity. A recent study by Motter et al. [8] showed that RC walls built to satisfy the new minimum vertical reinforcement provisions in the New Zealand Concrete Structures Standard (NZS) 3101:2006-A3 [9] could be repaired to reinstate the structural capacity after being subjected to extensive structural damage, but the invasive and costly repairs required may not be practical in damaged buildings.

In order to mitigate structural damage during an earthquake, engineers and researchers have developed alternative low-damage structural systems. For concrete structures, such systems have typically been based on the concept of rocking or jointed precast components tied together with unbonded post-tensioning [10]. These post-tensioned systems have been shown to provide satisfactory seismic performance

* Corresponding author.
E-mail addresses: stephen.blount99@gmail.com (S.W. Blount), klryan@unr.edu (K.L. Ryan), rs.henry@auckland.ac.nz (R.S. Henry), yiqiu.lu@auckland.ac.nz (Y. Lu), k.elwood@auckland.ac.nz (K.J. Elwood).
[1] Formerly of University of Nevada Reno.

https://doi.org/10.1016/j.engstruct.2019.110034
Received 10 April 2019; Received in revised form 27 November 2019; Accepted 1 December 2019

with minimal repair required following large earthquake demands. However, the design of post-tensioned rocking systems requires a significant change of the design philosophy and procedures, a factor that may limit uptake, particularly for ordinary buildings. On this basis, a long term objective for the engineering community is to develop of a variety of options to reduce expected earthquake damage that would suit different design and construction contexts.

A series of tests were conducted on walls with minor design modifications relative to conventional RC walls with the aim of improving their repairability following earthquake demands. For a conventional RC wall, modifications were considered that would limit the damage to reinforcing steel but reduce plastic strain demands (or localized strain demands) and prevent bar buckling, allowing for straightforward repairs using techniques such as epoxy injection of cracks. Marder et al. [11] has shown that modest repair techniques are effective to restore the deformation capacity, when applied to mildly damaged RC beams. For this study, a benchmark (BM) wall tested previously by Lu [12] was used for the wall design, with modifications consisting of debonding of reinforcement at the wall base (DBR wall), substituting fiber-reinforced concrete for conventional concrete (FRC wall), and substituting engineered cementitious composite (ECC) for conventional concrete in the ends of the plastic hinge regions (ECC walls). The performance of these modified walls was compared against the BM wall to assess their repairability following varying cycles of lateral in-plane drift, as well as their overall lateral strength, drift capacity, and failure mode.

2. Literature review

The use of unbonded post-tensioning to achieve self-centering and minimize structural damage has been extensively evaluated for concrete walls [10,13–16]. These walls utilize unbonded post-tensioning tendons that extend the height of the wall and are anchored at the base of the foundation. When subjected to lateral demands, the walls rock at the wall-to-foundation joint and exhibit recentering from the unbonded tendons. Different systems and configurations have been developed to incorporate additional energy dissipating devices, including the use of debonded vertical reinforcement at the wall base in addition to the post-tensioning tendons [17–19]. The detailing used in [17], which included steel armoring at the wall base, prevented visible damage from occurring for drift cycles out to 2.5%. Lu et al. [20] tested another concept closer to typical RC construction where conventional reinforcement was used through the central portion of the wall and steel plates formed slits at the wall ends where post-tensioning tendons were applied. Due to ease of construction compared to post-tensioned solutions, the use of debonded reinforcement in walls without the use of post-tensioning has been implemented in several buildings in New Zealand following the Canterbury Earthquakes [21] and the Structural Engineering Society promoted the use of debonded reinforcement for precast wall connections in their interim design guidance [22]. Such recommended debonding details have not been previously tested.

Significant research has focused on the use of alternative advanced cementitious materials for enhanced ductility of structural components to reduce damage and promote repairability. The introduction of fibers made of steel, glass or polymer into the matrix (i.e. FRC) has been investigated in a wide range of concrete mixes. Depending on the mix design and fiber type either a strain-softening or strain-hardening can be achieved. Strain hardening occurs when the fibers, which have a higher strength than the concrete, bridge and transfer stress across the cracks [23]. A critical volume ratio of fibers is needed to produce the strain hardening behavior [24], generally found to be on the order of 1.5% for steel fibers [25]. Tensile strain-hardening is enhanced through developments involving the matrix, the fibers, the fiber-matrix interface and the composite production process [26]. ECC, developed by Li and co-workers at University of Michigan, is a form of high performance fiber reinforced cementitious composite (HPFRCC) that is engineered for tensile ductility [27]. ECC uses synthetic polyvinyl alcohol (PVA) fibers or high modulus polyethylene (PE) fibers, added at 2% by volume ratio to the mix. The fibers are coated with a hydrophobic material that encourages them to slip and harden across the crack. The ECC tensile stress-strain curve phases up to failure are: elastic deformation to a strain of 0.01%, transition regime to a strain of about 1%, and strain hardening to strains of about 2–5%.

Advanced cementitious materials have been applied to numerous types of slender flexural (beam-column) members. Flexural members constructed with a strain-softening FRC display a decay in load carrying capacity reflecting crack localization immediately after first cracking; while with HPFRCC, the load carrying capacity increases after the point of first cracking and is generally accompanied by a multiple crack pattern with more uniform strain through the material [28]. Studies using regular FRCs in the plastic hinge regions for beam-column subassembly tests subjected to inelastic cyclic loading [29–31] have found the primary benefit to be relaxation of transverse reinforcement requirements. An HPFRCC with a tensile strain hardening capacity of 0.25–0.5% was evaluated in flexural members, joints and other applications [28,32–35]. HPFRCC was introduced mainly to allow simplification of transverse reinforcement detailing and improve constructability of reinforced-concrete shear critical components. HPFRCC with a tensile strain capacity of 2–5% was applied to the plastic hinge region of several columns [36]; the columns showed improved lateral load and deformation capacities and minimal cracks relative to a reference RC column. The self-confinement properties of ECC were also found to reduce/eliminate the need for transverse reinforcement and enhanced damage tolerance relative to conventional columns [37]. ECC was used to increase damage tolerance in the hinge region, reduce confinement, and enhance energy dissipation in post-tensioned segmented concrete columns [38]. Tests comparing multiple ECC mixes showed that performance was closely associated with tensile ductility [39].

Very promising results have been obtained in bridge columns by combining ECC and shape memory alloy (SMA) bars in place of conventional reinforcement in the column plastic hinge region [40–42]. SMAs are smart materials that undergo reversible solid-state phase transformation and can recover their initial shape upon removal of the applied stress, which is referred to as the superelastic effect. As a result, SMA displays a flag-shaped hysteretic stress-strain behavior, which tends to re-center the column. The self-confining and large strain capacity of ECC was found to be necessary to capitalize on the self-centering capabilities of the SMA bars.

Application of advanced materials to concrete walls has not been common, and HPFRCC/ECC and SMA bars have not been used in combination in flexural walls like they have in columns. HPFRCC was considered as a complete replacement for conventional concrete in low-rise walls with shear span ratios of 1.2 and 1.5 [43]. All the HPFRCC test walls incorporated relaxation of confining reinforcement in the boundary region, and exhibited slightly increased drift capacity and markedly reduced concrete spalling compared to reference code compliant RC walls. Furthermore, the use of HPFRCC was evaluated in the first two stories of coupled T-shape walls connected by coupling beams, again with relaxed confining reinforcement [35]. A shear-compression failure was observed in one of the walls at 2.5% drift. A concrete wall test incorporating SMA bars oriented diagonally along with conventional reinforcement was described in [44]. In a test comparing two walls with conventional reinforcement and SMA bars in the boundary region; SMA bars led to the recovery of 92% of the displacement versus 31% in the conventional wall [45]. Based on this literature review, a variety of approaches show promise for reducing damage in concrete flexural walls; a debonding detail and advanced cementitious materials were selected as the focus of this study.

3. Test walls

In this experimental program, four new RC walls were fabricated and tested to failure under a cyclic lateral loading protocol. The

Table 1
Description of test walls.

Wall	Description	Axial Load Ratio
Benchmark (BM)	Wall M5 tested by Lu [12]	$0.035A_g f'_c$
Debonded Reinforcement (DBR)	Vertical reinforcement was debonded at the wall base	$0.035A_g f'_c$
Fiber-Reinforced Concrete (FRC)	FRC with steel hooked fibers by 1% volume ratio was substituted for conventional concrete throughout	$0.035A_g f'_c$
Engineered Cementitious Composite (ECC)	ECC was substituted for conventional concrete in lower plastic hinge region at each wall end zone	$0.035A_g f'_c$
Engineered Cementitious Composite-High (ECC-H)	ECC was substituted for conventional concrete in lower plastic hinge region at each wall end zone	$0.064A_g f'_c$

dimensions and reinforcement details of the four new walls were identical to a benchmark (BM) wall evaluated in prior research. A design modification was applied to each new wall, and for one wall the applied axial load ratio was increased. The details of the BM wall and the four new walls are summarized in Table 1.

3.1. Benchmark (BM) wall

The BM wall was identified as wall M5 in prior experiments by Lu [12]. The M5 wall was part of a series of tests designed to investigate minimum vertical reinforcement limits. The wall was designed in accordance with new provisions, eventually adopted in NZS 3101:2006-A3 [5,9], that increased the minimum required vertical reinforcement in RC walls. Specifically, the provisions introduced a requirement for increased vertical reinforcement in boundary end zone regions extending at least $0.15l_w$ from each end, where l_w = wall length. The BM wall represented an approximately 40–50% scale version of lightly reinforced multi-story RC walls, with dimensions 2.8 m high, 1.4 m long, and 150 mm thick (Fig. 1). The wall was loaded to represent cantilever boundary conditions (no applied moment at the top) and thus had a

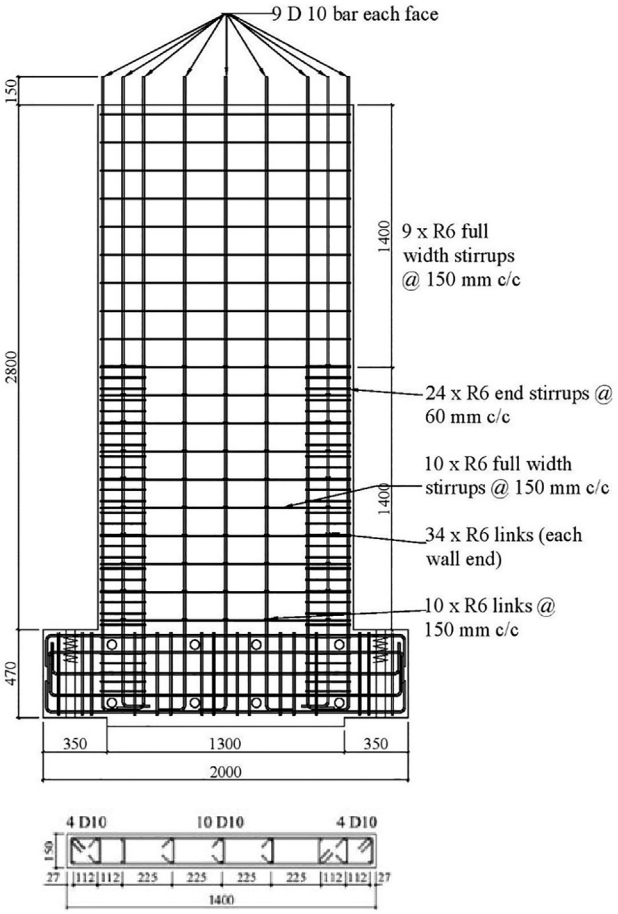

Fig. 1. BM wall design showing the reinforcement scheme.

shear span ratio of 2. The specified concrete strength (f_c') was 40 MPa and the specified yield strength of the steel reinforcement (f_y) was 300 MPa (commonly specified concrete and reinforcing grades in New Zealand). As per recent amendments to NZS 3101:2006, additional vertical reinforcement is required within the end zone of the wall section, defined as $0.15l_w$, or 210 mm. To meet required minimum vertical reinforcement requirements within the end zone, a group of four D10 (deformed 10 mm diameter) bars were required at either end of the walls, and D10 bars were spaced at 225 mm in the central web region. The resulting reinforcement ratios were 1% and 0.47% in the end zone and central web regions, respectively, compared to the minimum required ratios of 0.91% and 0.46%. Horizontal reinforcement consisted of R6 (plain 6 mm diameter) stirrups spaced at 150 mm over the entire wall height with additional R6 stirrups in the compression toe at a spacing of $6d_b$ (or 60 mm), to meet the ductile detailing provisions in NZS 3101:2006-A3. Cross ties were placed at stirrup locations over the lower half of the wall, as shown in Fig. 1. The baseline axial load was $0.035A_g f'_c$, where A_g = gross area of the wall cross section, which corresponded to an actual applied axial load of 294 kN. This axial load represents the lower end of the axial load demands expected in multi-story buildings with lightly reinforced walls. All subsequent walls were built with the same dimensions, shear span ratio, and reinforcement layout as the BM wall.

3.2. Debonded reinforcement (DBR) wall

Specimen DBR utilized debonding of the vertical reinforcement at the wall base to reduce strain localization at the wall-to-foundation region and to promote rocking about the base to minimize the number of cracks in the wall panel. The increased strain distribution was also expected to delay bar buckling and fracture of the reinforcement. All of the vertical reinforcement in the wall was debonded by placing a steel sleeve over the bar and sealing the ends, as shown in Figs. 2(a) and 3. The debonding sleeves were located in the foundation and terminated at the foundation-to-wall interface. Limiting the sleeves to the foundation was expected to protect the sleeves from loss of surrounding concrete due to spalling and crushing in the wall. Additionally, debonding the reinforcement in the wall panel may instead lead to the dominant crack opening above the wall base, which was not desired. The debonded length was 300 mm and was estimated to reduce the strains to less that 6% at a lateral wall drift of 1.5%, based on analysis of the wall as a rigid rocking block with plastic rotation about a single crack/joint at the wall base. Apart from the debonding sleeves, all other parameters for the DBR wall were consistent with that of the BM wall.

3.3. Fiber-Reinforced concrete (FRC) wall

For the FRC wall, Dramix 4D 65/60BG steel hooked fibers, 60 mm in length and 0.9 mm in diameter were mixed at 1.00% by volume ratio, throughout the entire batch of concrete with no other changes to the concrete mix. The mix represented standard medium volume ratio FRC mix readily available in New Zealand. The wall was otherwise identical to the BM wall. As discussed earlier, the steel fibers were intended to increase both compressive and tensile strength. The latter is achieved by steel fibers, which have a tensile strength (manufacturer specified 2300 MPa) that far exceeds that of the concrete, bridging open cracks.

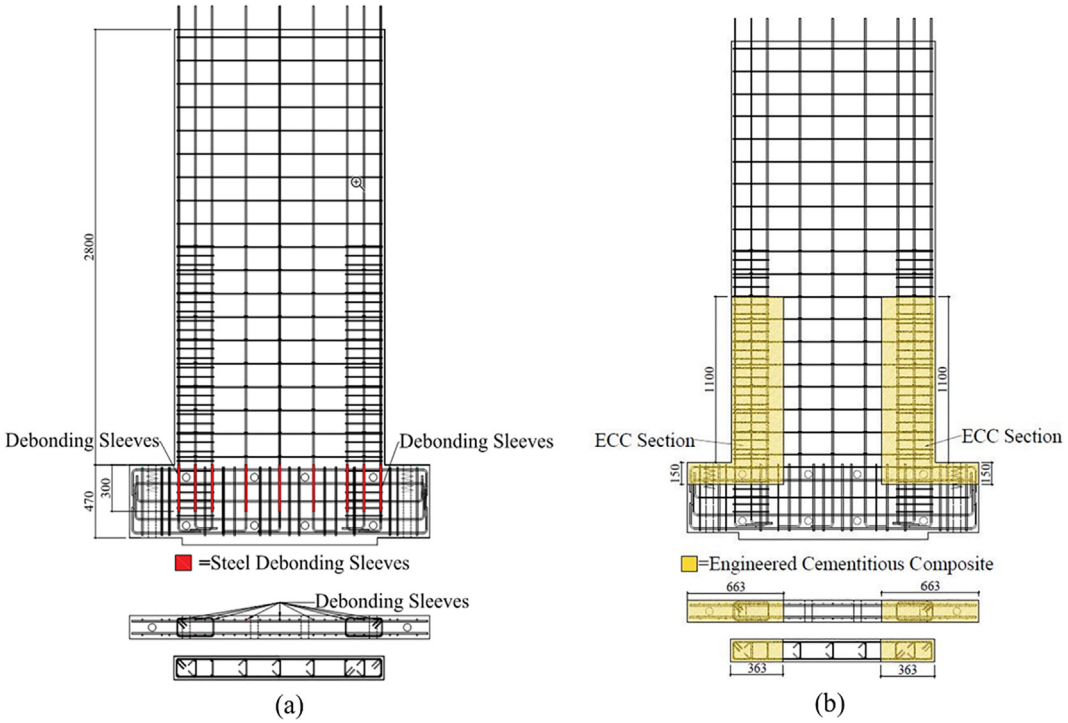

Fig. 2. Wall design schematics: (a) DBR wall, reinforcement and sleeves (shown in red), and (b) ECC wall, reinforcement and ECC cut outs (shaded). (For interpretation of the references to color in this figure legend, the reader is referred to the web version of this article.)

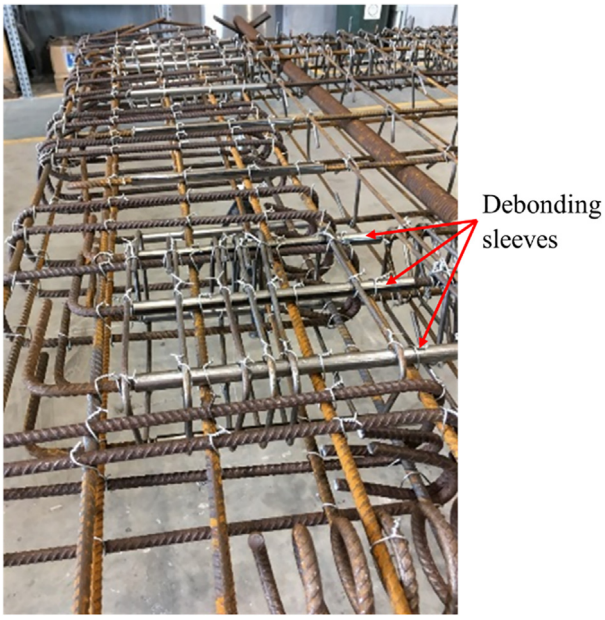

Fig. 3. Close-up of debonding sleeves in DBR wall.

Fig. 4 shows images of the dimensions and curvature of the Dramix 4D fibers, which are specifically engineered to have increased anchorage to prevent fiber pull out. The steel fibers also provide passive confinement, resisting the dilation that occurs when concrete is in compression.

3.4. Engineered cementitious composite (ECC) walls

For the last two walls, ECC was cast in the most critical lower end regions (boundary elements) within the wall (ECC cutouts). ECC was limited to the boundary elements to make this design modification more economical; outside the plastic hinge regions conventional 40 MPa concrete was used. As shown in Fig. 2(b), the ECC cutouts extended roughly 363 mm from the edge of either end of the wall toward the center and 1100 mm above the foundation. These dimensions were selected to ensure that the ECC covered the entire length of the wall in compression at the ultimate limit state and extended high enough to prevent a dominant crack from forming at the top interface. To prevent delamination of the ECC from the foundation, the ECC was also extended 150 mm into the wall foundation. The ECC used was cement composite that excluded coarse aggregate and included PVA fibers at a 2.0% by volume ratio. The construction of the two ECC walls was identical, and the only variation was that the ECC wall had an axial load of $0.035A_g f'_c$ (294 kN) equal to that of the BM wall and the axial load was increased to $0.064A_g f'_c$ (540 kN) for the ECC-H wall. The increased axial load was intended to increase the compression demands in the wall toe to examine the influence of the ECC on confinement, and allow for the effect of axial load on the self-centering response of the walls to be investigated.

The ECC walls were cast in two stages, first the conventional concrete was poured and cured, followed by the ECC. Fig. 5(a) depicts placement of the formwork to allow the concrete and ECC sections to be cast separately and in sequence. The boundary formwork of the ECC and concrete was painted with a set retarder to form a roughened joint surface. Fig. 5(b) depicts the wall 24 h after casting the concrete. Due to project timing constraints, ECC was cast 2 months later. Before casting the ECC, the conventional concrete was wetted to meet saturated surface-dry (SSD) conditions. This construction methodology was considered appropriate for a precast concrete wall panel. Although ECC is ideally suited to precast components where the mixing and placing can be conducted under controlled conditions, it is conceived that the wall could also be constructed insitu with the ECC potentially cast prior to the conventional concrete. The insitu construction methodology is considered to be similar to that implemented for the precast test wall and no significant change in the wall response is expected due to the construction sequence or method.

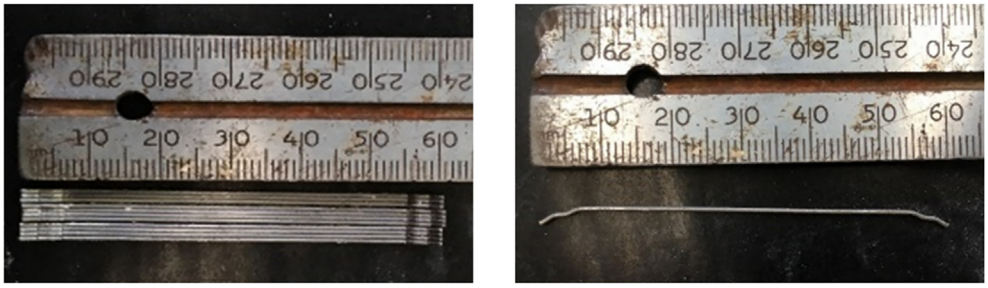

(a) (b)

Fig. 4. FRC wall: (a), (b) dimensional photos of steel hooked fibers.

3.5. Material properties

The steel reinforcement used in all test walls was specified to be G300E and was manufactured in accordance with AS/NZS 4671 [46]. Samples of the reinforcing steel were extracted from the supplied batches and three samples of each type of reinforcing bar were subjected to a direct tension test to confirm their stress–strain behavior. Strains in the test bars were measured over a 100 mm gauge length. Representative stress-strain curves from tensile tests of vertical (D10) reinforcement are shown in Fig. 6 for the BM wall and separately for the four modified walls, as the reinforcement for the two sets of walls came from different batches. The average properties determined from reinforcement samples (with standard deviations indicated in parentheses) are summarized in Table 2. Although the specifications were the same, the reinforcement for the BM wall had much higher yield (f_y) and ultimate strength (f_u), while the reinforcement in the modified walls had a larger ultimate strain (ε_u).

Six 100 mm diameter by 200 mm long concrete and ECC (as applicable) cylinders were cast for each wall specimen and the mechanical properties of those cylinders as measured on test day are listed in Table 2. Three cylinders were used for compression testing to obtain the average measured concrete compressive strength (f_{cm}) and three were used for a split cylinder test to calculate the average tensile strength (f_t). The average density (ρ_c) was also recorded using the dry weight and submerged weight of each specimen. These average properties are shown in Table 2, with standard deviations in parentheses. The FRC and ECC realized 25% and 50% increases in tensile strength compared to the conventional concrete, respectively. These increases in tensile strength can be attributed to the inclusion of fibers within the two mixes. Note that for ECC only, tensile strength was also obtained as the modulus of rupture from flexural beam tests (Table 2). The difference in conventional concrete compressive strength of the ECC walls compared to the other walls can be attributed to the extra three months of curing time available to the ECC walls; however, the strength of the conventional concrete was not expected to significantly influence the overall wall strength.

4. Test setup and loading protocol

The test setup shown in Fig. 7 was identical to that used for the BM wall and others in the same test series [5]. All walls were cast horizontally by a local precaster. Each wall was erected in the lab and grouted and post-tensioned horizontally between two concrete foundation blocks that were then post-tensioned to the strong floor. This setup was meant to mimic cast-in-place construction. Three actuators were used, one to apply the lateral load and two to apply the axial load. A shear span ratio of 2 was provided by keeping the axial load identical and constant in the two vertical actuators throughout each test, such that no moment was applied to the top of the walls.

The cyclic loading protocol used during the wall tests was also consistent with that applied to the walls in the prior test series [5]. Before commencement of the lateral loading on the walls, the constant

(a) (b)

Fig. 5. ECC wall construction: (a) formwork prior to casting, (b) partially cast wall.

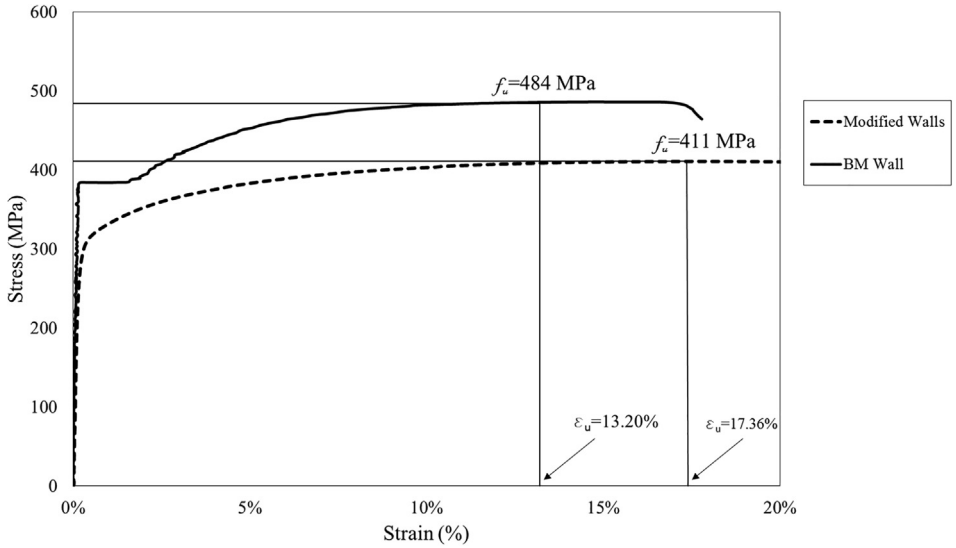

Fig. 6. Measured stress-strain of D10 reinforcing steel.

axial force was applied. Initially, four force-controlled cycles were applied, whereby the load was increased to the theoretical cracking moment at base of the wall in quarter steps. The remainder of the loading sequence was displacement-controlled, with three complete cycles at each increasing increment of drift. These cycles include lateral drifts of 0.20%, 0.25%, 0.35%, 0.50%, 0.75%, 1.00%, 1.50%, 2.00%, 2.50%, up to a maximum of 3.50%. Termination of wall tests was determined by the occurrence of wall failure.

4.1. Instrumentation

The instrumentation plan for the four new modified walls is shown in Fig. 8. The number of instruments were reduced slightly compared to the BM wall [12], since plasticity tends to concentrate at the base for walls with a shear span ratio of 2. The wall lateral displacement was measured by two string-pot displacement gauges attached at the top of the walls on each side. The displacements and forces of all three actuators were monitored by internal linear variable differential transformers (LVDT) and load cells, respectively. Average strains in the outer most vertical reinforcement were measured by four displacement gauges on either side, extending up the first meter of the wall height. These gauges were attached to metal studs that had been welded to the reinforcement prior to concrete pouring. Wall panel displacements were measured by nine displacement gauges that extended up the entire wall height at either end of the wall. These gauges were attached to steel studs that were inserted into the concrete roughly 30 mm from the wall edge. Shear deformations across the wall were measure by four displacement gauges set up in two "X" configurations, or shear grids, as shown in Fig. 8. Horizontal and vertical slip between the foundation-to-strong floor, foundation block-to-wall, and loading beam-to-wall connections were also measured by displacement gauges.

5. Results

5.1. Response at small drifts

Cracking was first observed in all walls during the first displacement controlled cycle at 0.20% drift, where numerous cracks developed on the lower half of each wall. The BM and FRC walls formed a small number of new secondary cracks during the second cycle at 0.20% drift, while in contrast both ECC walls developed a large number of new microcracks. Additional flexural cracks did not form in the DBR wall until the first cycle at 0.25% drift.

The crack distribution patterns and maximum crack widths at peak displacements were observed throughout the tests and compared in all walls to assess the spread of plasticity and repairability. Fig. 9 depicts crack maps for all walls at the common lateral drift of 0.50%. In these crack maps, the colors green and red represent cracks formed during drift cycles in the positive and negative directions, respectively. Table 3 summarizes for each wall the average number of cracks, associated crack spacing, and maximum crack width opening for loading up to 0.50%, which generally occurred at the peak positive or negative cycle. The average number of cracks was determined by counting the total number of cracks on the tension edge of the walls in Fig. 9 and dividing by the distance from the base to the top observed crack. Cracks greater than 0.1 mm thick were detected by visual inspection.

The more densely populated crack patterns, increased number of cracks and decreased crack spacing in FRC and especially ECC walls (Fig. 9, Table 3) indicated that up to 0.5% drift, the fiber reinforcement and special mix designs had the intended effects of preventing strain localization and distributing cracking evenly within the walls. The average crack spacing for the FRC and ECC walls was roughly 1.5 and 2.5 times smaller than the spacing reported for the BM wall,

Table 2
Overview of concrete and reinforcement characteristics.

Wall	Reinforcement			Concrete		ECC		
	f_y (MPa)	f_u (MPa)	ε_u (%)	f_{cm} (MPa)	f'_t (MPa)	f_{cm} (MPa)	f'_t Cylinder (MPa)	f'_t Beam (MPa)
BM	R6 = 322 D10 = 387	R6 = 450 D10 = 484	R6 = 16.4 D10 = 13.2	31.2	2.15	N/A	N/A	N/A
DBR	R6 = 340 (2.23)	R6 = 462 (2.64)	R6 = 15.0 (0.95)	35.8 (2.05)	3.19 (0.21)			
FRC	D10 = 314 (4.40)	D10 = 411 (0.97)	D10 = 17.4 (1.94)	38.6 (1.97)	3.95 (0.60)			
ECC				52.0 (1.08)	3.26 (0.50)	47.3 (2.46)	5.1 (0.07)	6.6 (0.93)
ECC-H				43.6 (1.75)	3.48 (0.24)	50.5 (0.78)	5.0 (0.28)	

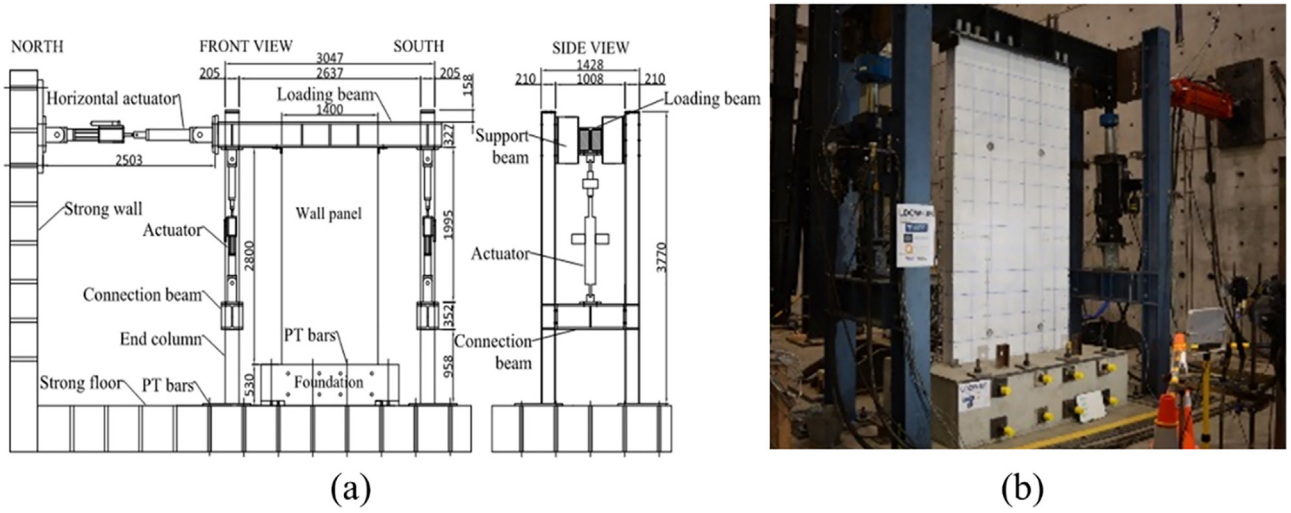

Fig. 7. Test setup: (a) drawing, and (b) photo of representative wall in the laboratory.

respectively. The inclusion of fibers was also shown to better control maximum crack widths when compared to the walls without fibers (Table 3). The total number of cracks for the ECC and FRC walls are considered underestimations. The walls were painted white prior to testing, and it is possible that some microcracks were too small to break through the paint. Since the DBR wall mimicked a rocking wall, the limited cracking can be attributed to the early localization of the intended dominant crack at the wall-to-foundation interface.

5.2. Response at large drifts and failure

To assess large drift response at later stages of the testing program, average curvatures and reinforcement strain distributions of all walls at 1.50% drift are compared in Fig. 10, where strains are accurate to ± 0.1%. As mentioned earlier, curvatures (computed from the difference in measured concrete strains at the two ends of the wall) and reinforcement strains represent average values across the predetermined gauge length and do not reflect expected concentrations in curvature and strain at individual cracks. Also, the bottom displacement gauge stud on the north face of the FRC wall detached from the concrete during the test, causing an erroneously large curvature reading across the bottom displacement gauge. One of the reinforcement gauge studs on the ECC wall detached during construction and the gauge lengths of the adjacent gauges were extended to compensate, affecting the distribution of reinforcement strain on the lower part of the wall. Both of these anomalies are depicted as dashed lines in Fig. 10.

During large drift cycles, the performance of the BM wall was controlled by 2–3 dominant flexural cracks, whereas the four modified walls each formed a single dominant flexural crack at or near the wall base (the exact location of the crack varied on each side of each wall). The localization of deformation at this dominant crack occurred shortly after the cycles to 0.5% for the FRC and ECC walls. The multiple dominant cracks in the BM wall led to a better distribution of curvature over the lower half of the wall at larger drifts compared to all of the

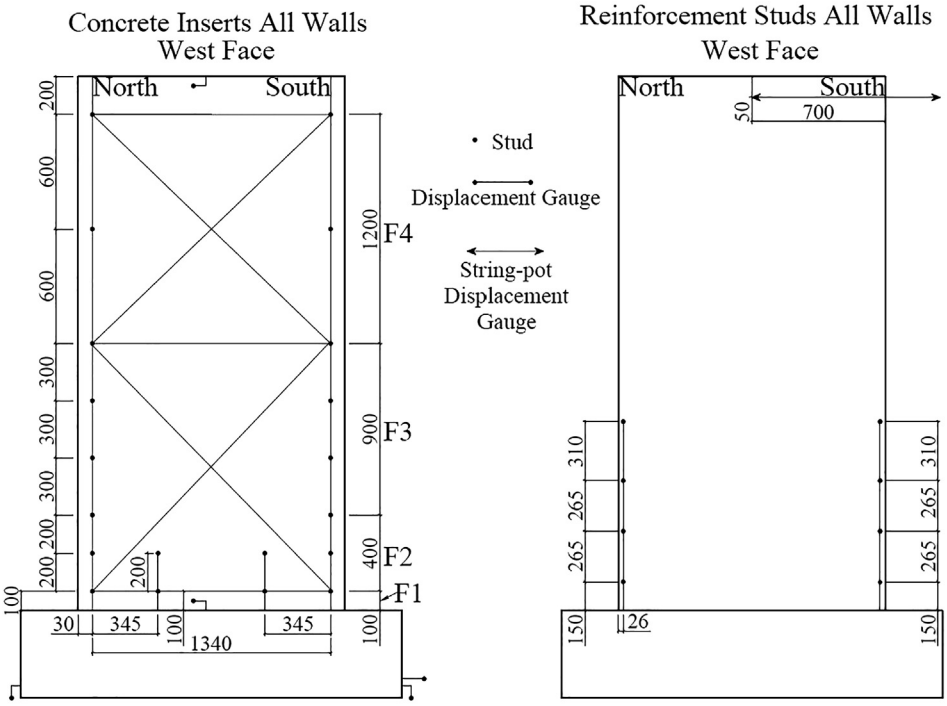

Fig. 8. Illustration of the wall instrumentation.

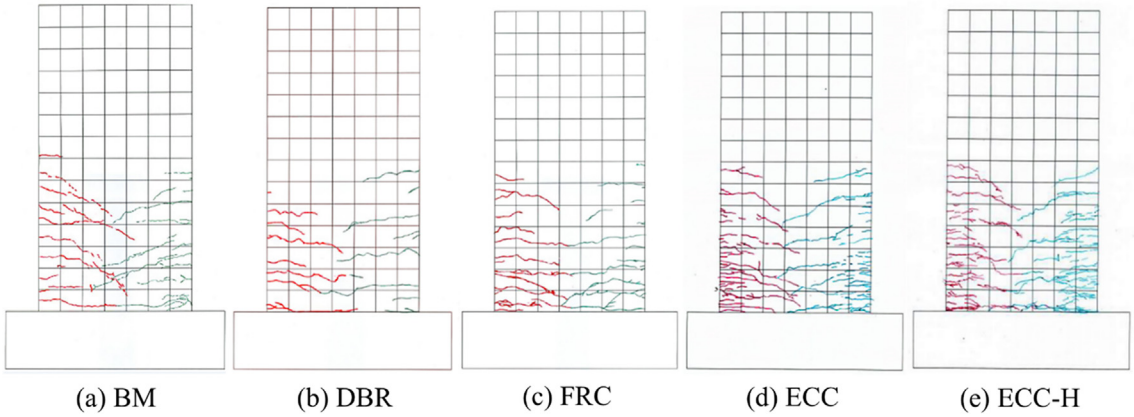

Fig. 9. Crack pattern maps at 0.50% drift.

Table 3
Average crack spacing and max crack width at 0.50% drift.

	Wall				
	BM	DBR	FRC	ECC	ECC-H
Average Number of Cracks	10	10	15.5	27.5	24
Average Crack Spacing (mm)	135	120	86	48	57
Maximum Crack Width (mm)	–*	3.3	1.5	2.3	1.7

* Maximum crack width information was not available for the BM wall.

Table 4
Observed buckling drift and associated reinforcement strain in all walls.

Test Wall	Drift at Bar Buckling (%)		Average Reinforcement Tensile Strain (%)	
	Drift to North	Drift to South	Drift to North	Drift to South
BM	+2.00%[3]	−1.50%[3]	4.3%	4.4%
DBR	−2.50%[3]	+2.00%[2]	6.2%	3.8%
FRC	−1.00%[3]	+1.50%[2]	3.6%	6.6%
ECC	–	−1.00%[3]	–	4.6%
ECC-H	−1.00%[1]	–	5.5%	–
	Average		4.9%	4.9%

Superscripts represent the cycle number.

modified wall designs (Fig. 10(a)). At a lateral drift of 1.50%, peak reinforcement strains were 3% in the DBR wall and 4% or higher in all other walls (Fig. 10(b)). For the FRC and ECC walls, the average strains were larger at the dominant base crack when compared to that of the BM wall where the plastic reinforcement strains were better distributed up the wall height. Debonding successfully reduced the reinforcement strains in the DBR wall at all drifts compared to the other walls, even though the base curvature was larger due to the rocking behavior.

As with the BM wall, buckling of the vertical reinforcement was observed in all test walls. The drifts at which bar buckling occurred and the measured reinforcement strains at these drifts are summarized in Table 4. The occurrence of reinforcement buckling for each wall was deduced by observed behaviors of visible distress, such as concrete spalling, bulging, or vertical cracks initiating in the vicinity of a buckled bar. The crack localization, or formation of a single dominant crack on each side, caused reinforcement buckling to occur prematurely in the FRC (1.0–1.5% drift) and ECC walls (1.0% drift) relative to the BM wall (1.5–2.0% drift). On the other hand, debonding was successful to delay buckling of vertical reinforcement in the DBR wall (2.0–2.5% drift) compared to the BM wall.

Fig. 11 shows the final condition of all test walls, including close-ups of the toe regions where damage was most concentrated. All five walls failed following bar buckling and subsequent fracture of the

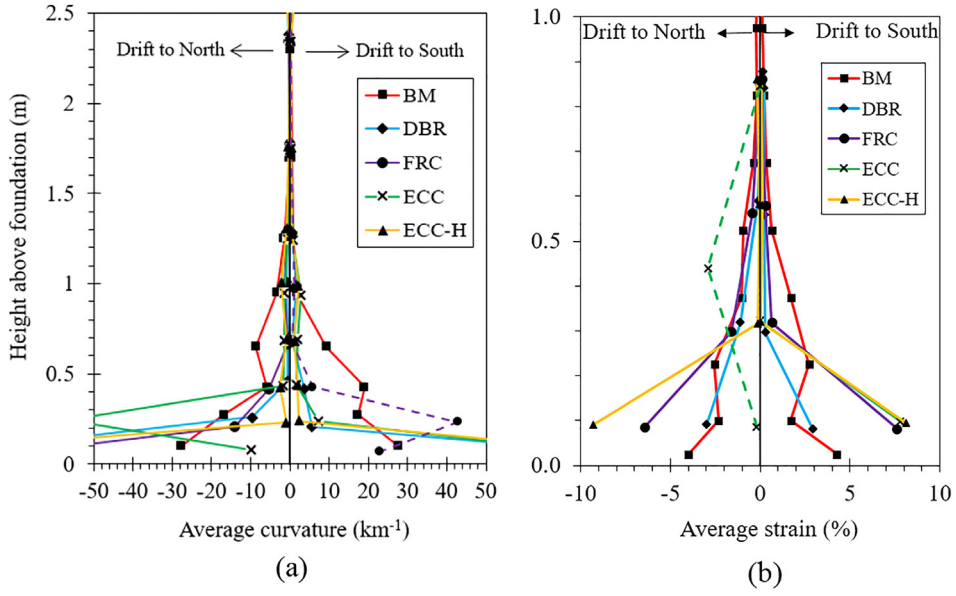

Fig. 10. Flexural demands at 1.50% drift for all walls: (a) average curvature and (b) average reinforcement strain.

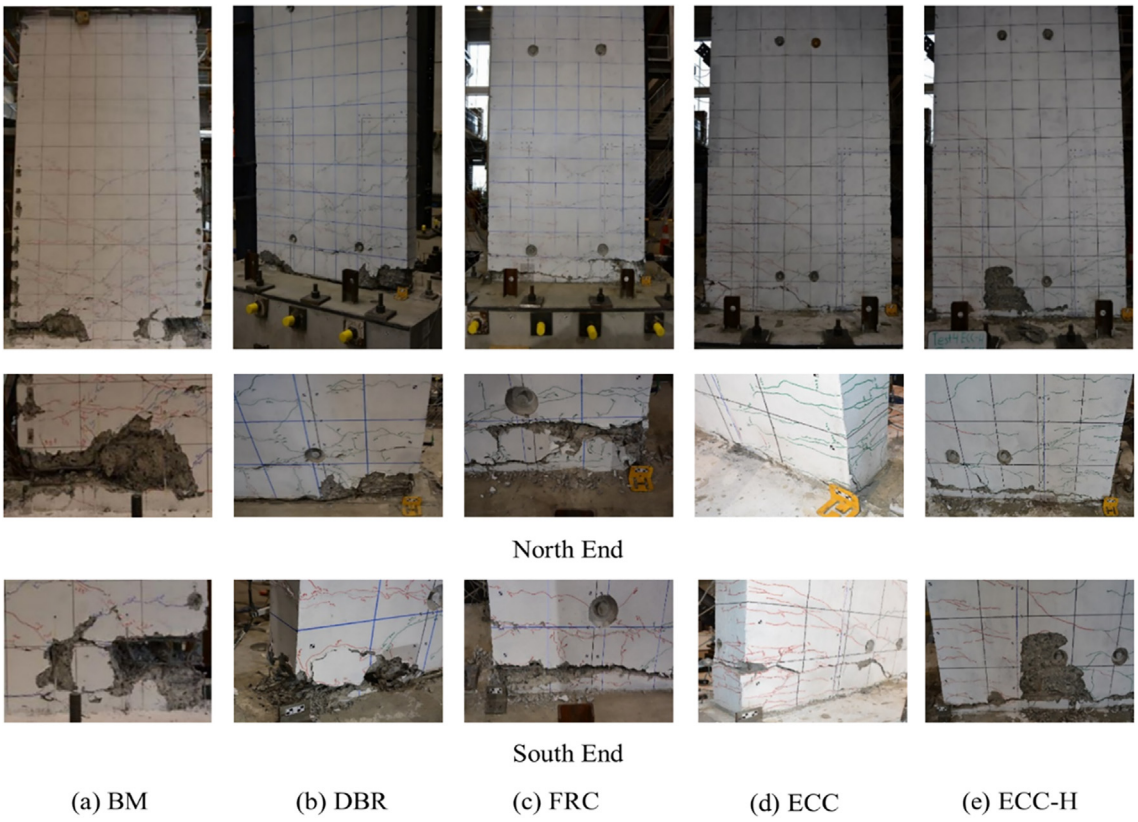

Fig. 11. Final condition of all test walls and exploded views of wall toes.

vertical reinforcement. The location of the single dominant crack can be seen in most of the walls. This crack did not always form directly at the wall base; for instance, the crack formed above the base at the north end of the FRC wall (Fig. 11(c)) and at the south end of the ECC wall (Fig. 11(d)). No significant spalling of ECC within the ECC walls was observed (Fig. 11(d) and (e)). However, the buckled reinforcement did start to push out the ECC cover at large drifts and significant spalling occurred in the central concrete region of the ECC-H wall (Fig. 11(e)).

For the DBR wall, a combination of bar buckling and wall sliding was observed during the later cycles of the test. The sliding of the wall at the base crack initiated during cycles to 2.5% drift and reached more than 15 mm to the south during cycles to 3.5% drift. While it was difficult to ascertain the exact sequence, buckling of the vertical reinforcement is believed to have occurred first, with the buckled bar constricted from freely sliding in the debonding tubes, preventing the closure of the base crack and leading to wall sliding. This conclusion is supported by results for previous test walls from which the BM wall was selected, where no wall sliding was observed despite dominant cracks at the wall base when an axial load of $0.035A_g f'_c$ was applied [5,20]. The wall sliding exacerbated the deformations on the buckled bars with fracture occurring during subsequent cycles.

The effects of the increased axial load on the wall can be seen from the photos in Fig. 11. The ECC and ECC-H walls had comparable amounts of degradation in the wall compression toe after the conclusion of testing, where the self-confining property of the ECC was effective in reducing the spalling and deterioration of the material even with the increase in the axial load. The larger compression demands in ECC-H did lead to additional spalling of the conventional concrete in the center of the wall directly adjacent to the ECC end region.

5.3. Complete test results

Table 5 summarizes the drifts at which first cracking, peak moment, concrete spalling, bar buckling, and bar fracture were observed; as well as the maximum moment capacity. The point of first cracking was similar for all walls regardless of design modifications. Comparatively, the cracking moment of the ECC-H wall was slightly higher than the others due to its increased axial load. Surface spalling occurred earliest in the FRC wall at the last drift cycle of 0.75% drift. The DBR wall began to spall at similar drift to the BM wall, while as mentioned previously, the ECC walls both had minimal spalling. Buckling of reinforcement in the FRC and ECC walls occurred at lower drifts compared to the BM wall and was delayed in the DBR wall relative to the BM wall.

The moment-displacement hysteresis response and related backbone curves are displayed in Figs. 12 and 13, respectively. The backbone curves in Fig. 13 were developed by plotting the values of moment and displacement at the first positive and negative peaks of each new drift cycle. The BM wall achieved its peak moment capacity at the first cycle of 1.5% drift. In comparison, the peak moment in the DBR wall was observed one full drift increment higher than the BM wall, while the FRC and ECC walls achieved peak moment capacity at drifts less than 1.0%. All walls gradually decreased in strength after bar buckling and became unstable after the point of bar fracture. Wall failure was characterized as the point where observed moment capacity dropped below 80% of the peak moment. Each failure point is indicated by a large dot on the corresponding backbone curves in Figs. 12 and 13, but the failure could have occurred in a subsequent cycle at the same drift. By this definition, the FRC and both ECC walls failed during the 1.5% drift cycle and the DBR and BM walls both failed during the second cycle of 2.5% drift. The DBR wall demonstrated better performance in the north loading direction with bar buckling and fracture occurring earlier at one end of the wall. This indicates that improved performance could be achieved relative to the BM wall if bar buckling and wall sliding are suppressed.

Residual drift, as a measure of the recentering capability of the walls, can be approximately interpreted from the hysteresis loops as the drift or displacement at zero force. For comparison, the residual drift of all walls at 1.5% peak drift were determined from the average of the

Table 5
Comparison of damage states and associated drifts.

Test Wall	Face	Drift Cycle @						Peak Moment (kN-m)
		First Cracking	Peak Moment	Concrete Spalling	Bar Buckling	Bar Fracture	Failure	
BM	N	+0.07%[1]	+1.50%[1]	+2.00%[1]	+2.00%[3]	+2.00%[3]	+2.50%[2]	635.5
	S	−0.05%[1]	−1.50%[1]	−1.50%[1]	−1.50%[3]	−2.50%[2]	−2.50%[2]	−615.2
DBR	N	+0.06%[1]	+2.00%[1]	−1.50%[1]	−2.50%[3]	+3.50%[3]	+3.50%[3]	540.4
	S	−0.05%[1]	−2.00%[1]	+2.00%[2]	+2.00%[2]	+2.00%[3]	−2.50%[2]	−572.1
FRC	N	+0.06%[1]	+0.75%[1]	+0.75%[3]	−1.00%[3]	+1.50%[3]	+1.50%[3]	605.2
	S	−0.03%[1]	−0.75%[1]	−0.75%[3]	+1.50%[2]	−2.00%[1]	−2.00%[2]	−618.1
ECC	N	+0.06%[1]	+0.50%[1]	–	–	+1.50%[3]	+1.50%[3]	603.6
	S	−0.05%[1]	−0.75%[1]	+1.50%[3]	−1.00%[3]	−1.50%[1]	−1.50%[1]	−688.0
ECC-H	N	+0.10%[1]	+0.50%[1]	–	−1.00%[1]	+1.50%[1]	+1.50%[2]	766.4
	S	−0.07%[1]	−1.00%[1]	−1.00%[3]	–	−1.00%[3]	−1.50%[2]	−759.0

*Superscripts represent the cycle number.

positive and negative drift cycles. The residual drift values are: BM = 0.90%, FRC = 0.83%, DBR = 0.93%, ECC = 0.73%, and ECC-H = 0.47%. The differences between the BM, FRC and DBR are correlated to slight differences in achieved peak drifts at the 1.5% target, and are deemed to be insignificant. The lower residual drift in the ECC wall is attributed somewhat to an imbalance in the hysteresis loops for positive and negative drift cycles (Fig. 12(d)); in fact, the ECC wall experienced rapid degradation of moment capacity on the negative drift cycle. In contrast, the ECC-H wall exhibited a notable increase in strength accompanied by reduced residual drift and more flag-shaped hysteresis. The lower residual displacements in the ECC-H wall could be a result of delayed tensile yielding at comparable drifts to the ECC wall; however, higher strain concentrations were observed in the ECC-H wall upon failure at 1.5% drift (as was shown in Fig. 10(b)). Nevertheless, the ECC-H wall maintained a more stable hysteresis response throughout the 1.5% drift cycle (Fig. 12(e)). Thus, if the other objectives of using ECC had been achieved, the increased axial load ratio would be of benefit in reducing residual drift.

From these curves and the observed peak moments (Table 5), the moment capacity of the DBR wall was roughly 20% less than that of the BM wall. This decrease in moment capacity primarily reflects (1) the reduction in reinforcement batch strength for all modified walls relative to the BM wall (Fig. 6), and (2) reduced plastic strains in the debonded reinforcement (Fig. 10(b)). Assuming that the strength reduction was dominated by the reinforcement strength, the peak moment capacity in the DBR wall can be considered a reference to evaluate the effect of advanced materials in the other walls. Therefore, increased moment capacity of ECC and FRC walls relative to the DBR wall reflects the increased compressive and tensile strength of the alternative cementitious materials. Thus, their moment capacity is expected to have exceeded that of the BM wall if comparable strength vertical reinforcement was used.

From the backbone curves, the FRC and both ECC walls experienced strength decay soon after crack localization occurred. This is characterized as a deformation softening response, which suggests the likelihood of a strain softening response of fibrous materials after the

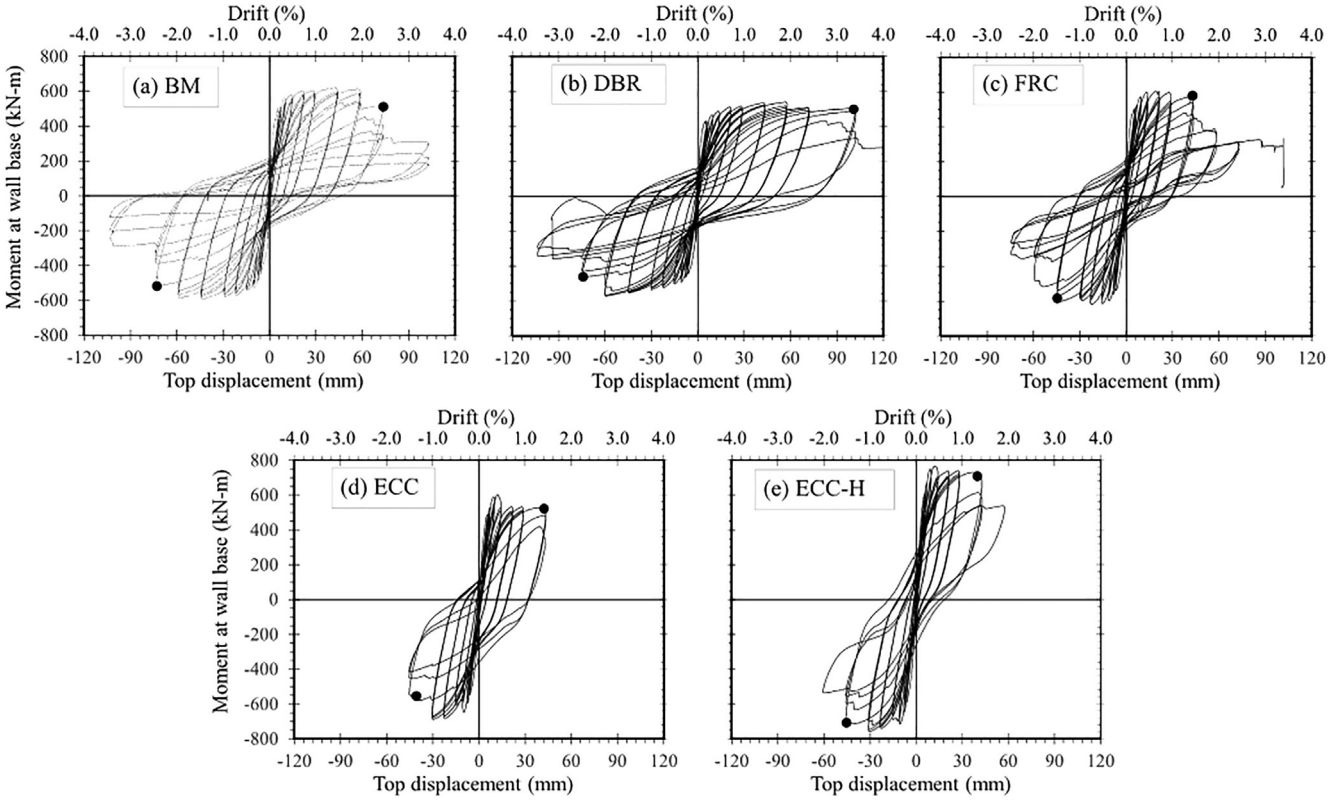

Fig. 12. Complete cyclic moment-displacement response for all test walls.

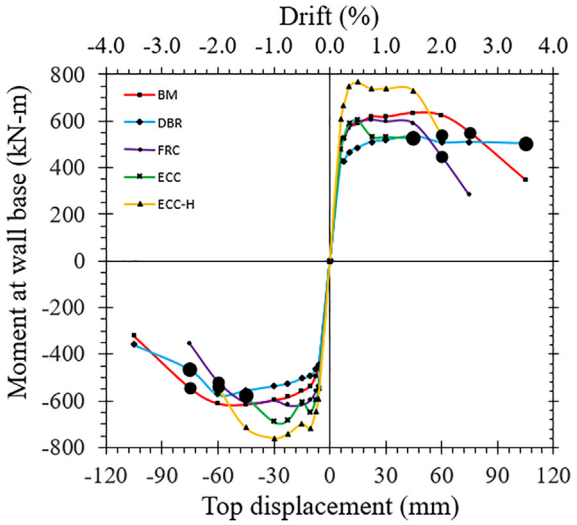

Fig. 13. Moment vs. displacement backbone curves for all five test walls.

point of crack localization. This deformation softening led to bar buckling and subsequent failure of the FRC and ECC walls at lower drifts than for the BM wall. Once peak moment capacity was achieved in these walls, the moment capacity decreased steadily until failure.

The deformation components for all walls computed at the first cycle of each new drift are plotted in Fig. 14. The contributions to total deformation in each wall were subdivided into five components: F1, F2, F3, F4 and shear. F1 to F4 represent flexural deformations attributed to regions of the wall panel, as labeled in Fig. 8, and were calculated by double-integrating the average curvature calculated from the displacement gauges at the edges of the wall panel. The shear deformations were calculated from the diagonal displacements across the shear grid in accordance with the method proposed by Hiraishi [47]. The deformation of each component was normalized by the total wall deformation recorded by a string-pot displacement gauge attached to the top of each wall. The average error between the summation of the total calculated deformations and the wall lateral deformation was generally within 10%, with some exceptions. For example, in the FRC and ECC walls, the dominant crack that opened on one side above the wall base was located within the lower shear grid, causing an increased rigid body motion within the grid. This motion artificially increased the computed shear deformation at the ends of the walls, increasing the summation of the five deformation components far beyond the total deformation measured from the string-pot displacement gauge.

In general, the wall responses were controlled by flexural deformations, with only minor shear deformations calculated for all walls. The BM wall formed 2–3 dominant flexural cracks, which allowed the flexural deformations to distribute over several of the flexural components F1 to F4. In the DBR wall, which was intended to mimic a rocking wall, a dominant base crack was observed early in the test, and thus the F1 flexural component at the wall base comprised most of the total flexural deformation at all drift levels. In the FRC and both ECC walls, the dominant flexural crack was not confined to the bottom of the wall (F1), but rather extended from the F1 section up to the F2 section on the side of the wall where the dominant crack formed above the base. In the FRC and ECC walls the relative contributions of deformation in the F1 and F2 components increased linearly with increasing drift, depending on where the dominant crack occurred. This correlated well with the observed behaviors of the walls: flexural deformation was spread over the wall height at the beginning of the tests and eventually localized to one flexural crack, which grew in width at every increased drift cycle.

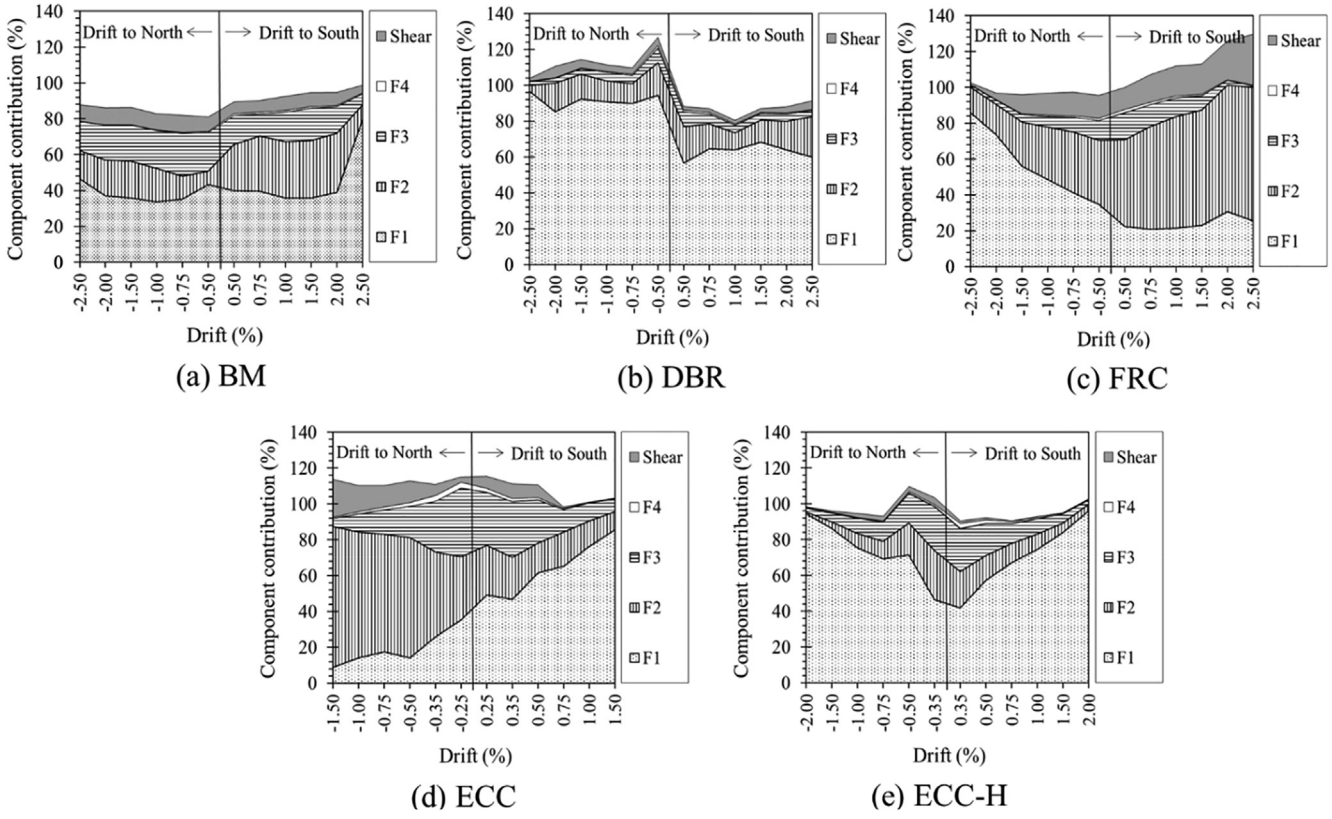

Fig. 14. Relative contribution of flexural (F1 to F4) and shear deformations in all walls.

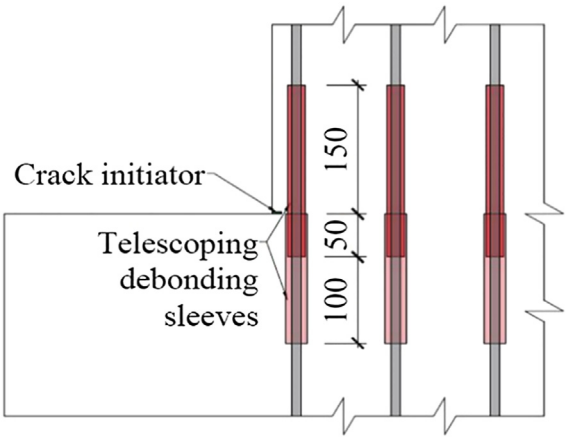

Fig. 15. Proposed design for new debonding mechanism.

6. Discussion and recommendations

6.1. Debonding detail

As expected, the DBR wall formed only one dominant base crack, and as the drift increased a large gap opened at the base crack. The DBR wall successfully distributed the vertical reinforcement strain along the length of the debonding sleeve. Despite this promising early performance, the vertical reinforcement buckled and the wall slid due to the buckled reinforcement being constrained from freely entering the debonding sleeve during load reversals. The buckling and shear deformation of the vertical reinforcement was severe, and fracture immediately ensued during subsequent cycles. The tested detail was chosen to be inexpensive and simple to construct. However, it is recommended that alternative detailing be adopted to better protect the vertical reinforcement from buckling and severe dowel action. One approach would be to substitute a thick layer of tape for the stiff steel sleeve, which has been successfully used for debonding bars in other tests and would prevent the bar getting caught on the sleeve. Another more complex alternative, shown in Fig. 15, involves using a second debonding sleeve located above the foundation that extends 50 mm into the foundation to act as a shear key. The sleeve from the foundation would be sized to fit around the wall sleeve and allow the sleeves to move relative to each other while the bar remains protected inside. To prevent the dominant crack forming at the top of the wall sleeve, a crack inducer (slit in the wall or plastic sheet) may be required at the wall-to-foundation interface.

6.2. FRC and ECC mixes

Both the FRC wall and ECC walls initially propagated a larger number of secondary cracks and achieved a peak moment strength comparable to the BM wall despite the reinforcing steel being 20% weaker. However, localization to a single dominant crack occurred in these walls at premature drifts, shortly after 0.50%, thus leading to reinforcement buckling and failure at lower drifts than in the BM wall. The performance suggests that these fiber-reinforced materials, especially ECC, did not exhibit the desired tensile strain hardening. While somewhat surprising that the large drift performance of these walls actually declined relative to the BM wall, an increased brittle failure mode is a known consequence of increasing concrete tensile strength without enhanced ductility. Once the fibers had failed or pulled out, the tensile strength of the vertical reinforcement at the dominant crack is less than that of the remainder of the panel where the fibers are still bridging cracks. The isolation of deformations at the base crack in the ECC walls was similar to that observed for comparable RC walls with less vertical reinforcement [48], where the quantity of vertical reinforcement is insufficient to overcome the concrete tensile strength to generate additional secondary cracks.

In the FRC walls, the steel Dramix fibers were observed to have pulled out from the concrete at the dominant crack. This is counter to the design objective where the fiber anchorage is intended to be sufficient to develop the full tensile capacity of the fiber. It is possible that the cyclic loading affected the performance of the FRC. The damage sustained when the wall toe was subjected to compression may have weakened the FRC concrete (e.g. micro-cracking) and resulted in premature pull out of the fibers when subjected to tension cycles. Additionally, the fibers were added at approximately 1% by volume ratio to the mix and increasing the fiber content to 2% by volume may lead to improved tensile ductility/strain hardening within the material. Some authorities caution that adding steel fibers greater than 1.5% by volume ratio may reduce the workability of the concrete mix and cause clumping; however, high fiber content may be used with special fiber addition techniques and placement procedures [49].

With regard to the ECC, the method of mixing the materials may have influenced the material properties and a seeming lack of tensile ductility compared to what has been achieved in many other tests. The best practice recommended by the supplier is to mix the ECC with a high shear mixer, such as a mortar mixer, until it reaches a thick non-spreadable paste-like substance. However, a mortar mixer was not readily available to the researchers for this project. In such circumstances, the supplier indicated that the desired mix properties can also be attained by mixing the ECC in buckets using a drill. However, when mixed with a drill, the material properties are much more susceptible to variation stemming from drill attributes (e.g. power and speed of the drill, shape and surface area of the paddle attached to the drill), as well as human factors (time and thoroughness of hand mixing). Thus, these factors may have contributed to the ECC mix falling short of the maximum achievable tensile ductility. On the other hand, given geometric differences between walls and columns, the strain demands in the tested walls may have been larger than columns at respective large drifts, making the concrete wall a less suitable application for a substitute plastic hinge using advanced materials. Finally, past studies [40–42] have observed very good performance of columns with ECC hinge zones especially when combined with SMA reinforcement. Combining the ECC with SMA reinforcement or debonded reinforcement may also improve the wall response. Further research is recommended to determine how to best apply ECC in flexural walls to take advantage of the self-confining and tensile ductility features.

7. Conclusions

Potential design modifications to conventional reinforced concrete walls that would lead to enhanced repairability were evaluated. Four new walls were constructed and subjected to cyclic loading to failure. The modifications considered included: debonding reinforcement at the wall base (DBR wall), substituting fiber-reinforced concrete for conventional concrete (FRC wall), and substituting engineered cementitious composite (ECC) for conventional concrete in the plastic hinge end region, which was applied at the reference axial load (ECC wall) and a higher axial load (ECC-H wall). Besides the stated modifications, the new walls had the same geometry, reinforcement scheme, and specified material properties as a previously tested BM wall. These wall tests have led to the following conclusions:

- The BM wall developed the most even distribution of curvature and reinforcement strain over the wall height due to the formation of multiple dominant flexural cracks. Reinforcement buckling and significant spalling were observed at 1.5–2% drift, bar fracture was observed at 2–2.5% drift, and the wall was considered failed at 2.5% drift.
- Debonding of reinforcement in the DBR wall reduced the peak reinforcement strains and delayed bar buckling (2–2.5% drift) relative

to the BM wall by distributing the reinforcement strain over the length of the debonding sleeve. Buckling of the reinforcement was followed by sliding at the wall base as the deformed shape prevented the bar retracting freely into the sleeve. The buckling led to reinforcement fracture during the following drift cycle, and thus wall failure occurred at the same drift (2.5%) as the BM wall.

- Relative to the BM wall, the FRC and both ECC walls had increased crack propagation up to a drift demand of 0.5% due to the addition of the fibers. However, the performance of these walls fell short of expectations as crack localization began to occur shortly after 0.5% drift, with a single dominant crack forming. This behavior led to early reinforcement buckling (1–1.5% drift) and subsequent failure (1.5% drift) compared to the BM wall.

At this stage, the design modifications considered are not found to be ready for application in flexural walls. The following ideas should be explored to better understand the potential for the lower damage modifications to improve performance relative to the conventional wall. First, for the DBR wall, an overlapping double sleeve debonding detail (Fig. 15) along with crack initiators should be considered for better protection against reinforcement buckling and dowel action. For the FRC wall, the effect of cyclic loading should be investigated and the fiber volume ratio increased to 2% to provide improved tensile strain hardening. For the ECC walls, the influence of mix method (hand mix versus high shear mixer) on the material properties, in particular tensile ductility, should be quantified; and the suitability of ECC to enhance the ductility of concrete walls should be evaluated through modeling.

Declaration of Competing Interest

The authors declare that they have no known competing financial interests or personal relationships that could have appeared to influence the work reported in this paper.

Acknowledgements

This project was supported by QuakeCoRE, a New Zealand Tertiary Education Commission-funded Centre. This is QuakeCoRE publication number 0294. Additional funding was provided by the Building Performance Branch of the New Zealand Ministry of Business, Innovation and Employment (MBIE). The authors would also like to acknowledge the following companies and individuals provided support to the project: Fiber Matrix of Sparks, NV who supplied the ECC; Wilco Precast of New Zealand who manufactured the test walls; industry advisors Nic Brooke and Craig Stephenson; UoA structures lab staff Lucas Hogan, Jay Naidoo, Ross Reichardt, Mark Byrami, Andrew Virtue, and Shane Smith; and Zhibin Li who assisted with the tests.

Appendix A. Supplementary material

Supplementary data to this article can be found online at https://doi.org/10.1016/j.engstruct.2019.110034.

References

[1] Henry RS, Dizhur D, Elwood KJ, Hare J, Brunsdon D. Damage to concrete buildings with precast floors during the 2016 Kaikoura Earthquake. Bull NZ Soc Earthq Eng 2017;50(2):174–86.
[2] Kam WY, Pampanin S, Elwood K. Seismic performance of reinforced concrete buildings in the 22 February Christchurch (Lyttelton) Earthquake. Bull NZ Soc Earthq Eng 2011;44(4):239–78.
[3] Sritharan S, Beyer K, Henry RS, Chai YH, Kowalsky M, Bull D. Understanding poor seismic performance of concrete walls and design implications. Earthq Spectra 2014;30(1):307–34.
[4] Dashti F, Dhakal RP, Pampanin S. Tests on slender ductile structural walls designed according to New Zealand Standard. Bull NZ Soc Earthq Eng 2017;50(4):504–16.
[5] Lu Y, Gultom R, Ma QT, Henry RS. Experimental validation of minimum vertical reinforcement requirements for ductile concrete walls. ACI Struct J 2018;115(4):1115–30.
[6] Shegay A, Motter CJ, Henry RS, Lehman DE, Lowes LN, Elwood KJ. Impact of axial load ratio on the seismic response of planar walls. J Struct Eng 2018;144(8):04018124.
[7] Marquis F, Kim JJ, Elwood KJ, Chang SE. Understanding post-earthquake decisions on multi-storey concrete buildings in Christchurch New Zealand. Bull Earthq Eng 2017;15(2):731–58.
[8] Motter CJ, Clauson A, Petch J, Hube M, Henry RS, Elwood KJ. Seismic performance of repaired lightly reinforced concrete walls. Bull NZ Soc Earthq Eng 2017;50(4):574–85.
[9] NZS 301:2006-A3. Concrete structures standard (Amendment 3). Wellington, New Zealand: Standards New Zealand; 2017.
[10] Priestley MJN, Sritharan SS, Conley JR, Pampanin S. Preliminary results and conclusions from the PRESSS five-story precast concrete test building. PCI J 1999;44(6):42–67.
[11] Marder K, Motter C, Elwood KJ, Clifton GC. Testing of 17 identical ductile reinforced concrete beams with various loading protocols and boundary conditions. Earthq Spectra 2018;34(3):1025–49.
[12] Lu Y. Seismic design of lightly reinforced concrete walls PhD Dissertation University of Auckland; 2017
[13] Kurama Y, Sause R, Pessiki S, Lu LW. Lateral load behavior and seismic design of unbonded post-tensioned precast concrete walls. ACI Struct. J 1999;96(4):622–32.
[14] Perez FJ, Pessiki S, Sause R. Experimental lateral load response of unbonded post-tensioned precast concrete walls. ACI Struct J 2013;110(6):1045–55.
[15] Sritharan S, Aaleti S, Henry RS, Liu KY, Tsai KC. Precast concrete wall with end columns (PreWEC) for seismic resistant design. Earthq Eng Struct Dyn 2015;44(12):2075–92.
[16] Nazari M, Sritharan S, Aaleti S. Single precast concrete rocking walls as earthquake force-resisting elements. Earthq Eng Struct Dyn 2017;46(5):753–69.
[17] Holden T, Restrepo J, Mander J. Seismic performance of precast reinforced and prestressed concrete walls. J Struct Eng 2003;129(3):286–96.
[18] Restrepo J, Rahman A. Seismic performance of self-centering structural walls incorporating energy dissipators. J Struct Eng 2007;133(11):1560–70.
[19] Smith B, Kurama Y, McGinnis M. Design and measured behavior of a hybrid precast concrete wall specimen for seismic regions. J Struct Eng 2011;137(10):1052–62.
[20] Lu X, Dang X, Qian J, Zhou Y, Jiang H. Experimental study of self-centering shear walls with horizontal bottom slits. J Struct Eng 2017;143(3):04016183.
[21] Thornton AW, Cattanach AG. One Market Lane – seismic design post Canterbury. Proceedings of the 2013 NZSEE annual conference, Wellington, April 26–28. 2013.
[22] SESOC. Interim design guidance – design of conventional structural systems following the Canterbury earthquakes". New Zealand Structural Engineering Society. Version 9; 2013. Retrieved from: http://www.sesoc.org.nz/Design-Guides/SESOC-Interim-Design-Guidance-0.9.pdf.
[23] Afroughsabet V, Biolzi L, Ozbakkaloglu T. High-performance fiber-reinforced concrete: a review. J Mater Sci 2016;51(14):6517–51.
[24] Naaman AE, Reinhardt HW. Characterization of high performance fiber reinforced cement composites—HPFRCC. In: Naaman AE, Reinhardt HW, editors. High performance fiber reinforced cement composites 2 (HPFRCC 2), proceedings of the second international RILEM workshop. Cachan Cedex, France: RILEM Publications, s.a.r.l.; 1996. p. 1–24.
[25] Naaman AE. Strain hardening and deflection hardening fiber reinforced cement composites. HPFRCC 4 RILEM PRO 30, June. 2003. p. 95–113.
[26] Liao W-C, Chao S-H, Park S-Y, Naaman AE. Self-consolidating high-performance fiber-reinforced concrete (SCHPFRC)—preliminary investigation Rep. No. UMCEE 06-02 Ann Arbor, MI: Univ. of Michigan; 2006.
[27] Li VC. Can concrete be bendable? Am Sci 2012;100(6):484–93.
[28] Parra-Montesinos GJ, Chompreda P. Deformation capacity and shear strength of fiber-reinforced cement composite flexural members subjected to displacement reversals. J Struct Eng 2007;133(3):421–31.
[29] Gefken PR, Ramey MR. Increased joint hoop spacing in type 2 seismic joints using fiber reinforced concrete. ACI Struct J 1989;86(2):168–72.
[30] Filiatrault A, Pineau S, Houde J. Seismic behavior of steel-fiber reinforced concrete interior beam-column joints. ACI Struct J 1995;92(5):543–52.
[31] Bayasi Z, Gebman M. Reduction of lateral reinforcement in seismic beam-column connection via application of steel fibers. ACI Struct J 2002;99(6):772–80.
[32] Xia Z, Naaman AE. Behavior and modeling of infill fiber-reinforced concrete damper element for steel-concrete shear wall. ACI Struct J 2002;99(6):727–39.
[33] Parra-Montesinos GJ, Peterfreund SW, Chao SH. Highly damage-tolerant beam-column joints through use of high performance fiber-reinforced cement composites. ACI Struct J 2005;102(3):487–95.
[34] Canbolat BA, Parra-Montesinos GJ, Wight JK. Experimental study on seismic behavior of high-performance fiber-reinforced cement composite coupling beams. ACI Struct J 2005;102(1):159–66.
[35] Lequesne R, Parra-Montesinos G, Wight J. Seismic behavior and detailing of high-performance fiber-reinforced concrete coupling beams and coupled wall systems. J Struct Eng 2013;139(8):1362–70.
[36] Cho CG, Kim Y-Y, Feo L, Hui D. Cyclic responses of reinforced concrete composite columns strengthened in the plastic hinge region by HPFRC mortar. Compos Struct 2012;94(7):2246–53.
[37] Fischer G, Li VC. Effect of matrix ductility on deformation behavior of steel reinforced ECC flexural members under reversed cyclic loading conditions. ACI Struct J 2002;99(6):781–90.
[38] Billington SL, Yoon JK. Cyclic response of precast bridge columns with ductile fiber-reinforced concrete. J Bridge Eng 2004;9(4):353–63.
[39] Lee WK, Billington SL. Simulation of self-centering fiber-reinforced concrete columns. Proc ICE Eng Comput Mech 2008;161(2):77–84.
[40] Saiidi MS, O'Brien M, Zadeh M. Cyclic response of concrete bridge columns using

superelastic nitinol and bendable concrete. ACI Struct J 2009;106:69–77.
[41] Cruz Noguez CA, Saiidi MS. Shake table studies of a four-span bridge model with advanced materials. J. Struct Eng 2012;138(2):183–91.
[42] Varela S, Saiidi MS. Experimental study on seismically resilient two-span bridge models designed for disassembly. J. Earthq Eng 2019;23(1):72–111.
[43] Athanasopoulou A, Parra-Montesinos G. Experimental study on the seismic behavior of high performance fiber-reinforced concrete low-rise walls. ACI Struct J 2013;110(5):767–77.
[44] Liao WI, Effendy E, Song G, Mo YL, Hsu TTC, et al. Effect of SMA bars on cyclic behaviour of low-rise shear walls. Proc. SPIE6174, smart structures and materials: sensors and smart structures technologies for civil, mechanical, and aerospace systems. 2006. p. 61743H.
[45] Abdulridha A, Palermo D. Behaviour and modelling of hybrid SMA-steel reinforced concrete slender shear wall. Eng Struct 2017;147:77–89.
[46] Standards Australia (AS) and Standards New Zealand (NZS). Steel reinforcing materials. Sydney, Australia and Wellington, New Zealand: AS/NZS 4671; 2001.
[47] Hiraishi H. Evaluation of shear and flexural deformations of flexural type shear walls. Bull NZ Soc Earthq Eng 1984;46(2):88–96.
[48] Lu Y, Henry RS, Gultom R, Ma QT. Cyclic testing of reinforced concrete walls with distributed minimum vertical reinforcement. J Struct Eng 2017;143(5):04016225.
[49] Soufeiani L, Raman SN, Jumaat MZB, Alengaram UJ, Ghadyani G, Mendis P. Influences of the volume fraction and shape of steel fibers on fiber-reinforced concrete subjected to dynamic loading – a review. Eng Struct 2016;124:405–17.